

GRANAT/SIGMA Observation of the Early Afterglow from GRB 920723 in Soft Gamma-Rays

R. A. Burenin^{1,2}, A. A. Vikhlinin¹, M. R. Gilfanov^{1,3}, O. V. Terekhov^{1,2}, A. Yu. Tkachenko^{1,2}, S. Yu. Sazonov^{1,2}, E. M. Churazov^{1,3}, R. A. Sunyaev^{1,3}, P. Goldoni⁴, A. Claret⁴, A. Goldwurm⁴, J. Paul⁴, J. P. Roques⁵, E. Jourdain⁵, F. Pelaez⁶, G. Vedrenne⁵

¹ Space Research Institute, Russian Academy of Sciences, Profsoyuznaya 84/32, 117810 Moscow, Russia

² visiting Max-Planck-Institut für Astrophysik

³ Max-Planck-Institut für Astrophysik, Karl-Schwarzschild-Str. 1, 85740 Garching bei Munchen, Germany

⁴ CEA/DSM/DAPNIA/SAP, Centre d'Etudes de Saclay, 91191, Gif-sur-Yvette, Cedex, France

⁵ Centre d'Etude Spatiale des Rayonnements (CNRS/UPS) 9, avenue du Colonel Roche, BP 4346 31028 Toulouse Cedex, France

⁶ Department of Physics and Astronomy, Mississippi State University, MS 39762

the date of receipt and acceptance should be inserted later

Abstract. We present a GRANAT/SIGMA observation of the soft gamma-ray afterglow immediately after GRB 920723. The main burst is very bright. After ~ 6 s, the burst light curve makes a smooth transition into an afterglow where flux decays as $t^{-0.7}$. The power-law decay lasts for at least 1000 s; beyond this time, the afterglow emission is lost in the background fluctuations. At least $\sim 20\%$ of main burst energy is emitted in the afterglow. At approximately ~ 6 s after the trigger, we also observe an abrupt change in the burst spectrum. At $t < 6$ s, the ratio of 8–20 and 75–200 keV fluxes corresponds to the power law spectral index $\alpha = 0.0–0.3$. At $t = 6$ s, the value of α increases to $\alpha \approx 1$ and stays at this level afterwards. The observed afterglow characteristics are discussed in connection with the relativistic fireball model of gamma-ray bursts.

Key words: Gamma rays: bursts

1. Introduction

Fast and accurate localizations of gamma-ray bursts by *Beppo-SAX* helped to establish the connection of GRB with the sources of decaying X-ray, optical, and radio emission (e.g. Costa et al. 1997, Van Paradijs et al. 1997, Frail et al. 1997). X-ray afterglows were found in 15 of 19 well-localized bursts; in most cases, the X-ray flux decayed as a power law of time, $t^{-\beta}$, with β ranging from -1.1 (GRB 970508, Piro et al. 1998) to -1.57 (GRB 970402, Nicastro et al. 1998). The power law decay of flux also is observed in the optical (e.g. Wijers et al. 1997, Sokolov et al. 1998). This is a characteristic prediction of the relativistic fireball model of GRB (Mészáros, Rees 1993, Mészáros 1997, Waxman 1997, Sari et al. 1998). Indeed, the energy release in some GRB is enormous and sufficient to power the relativistic fireball (Kulkarni et al. 1998). The fireball observations immediately after the burst, when the temperature and density are at maximum, are of great interest. Un-

fortunately, it has been impossible to observe the afterglows in the radio, optical, or X-rays earlier than approximately 10 hours after the burst.

Some earlier observations indicated that the afterglows could immediately follow some GRB. There were detections of X-ray emission lasting for tens of seconds after the main burst was finished in gamma-rays (Sunyaev et al. 1990, Murakami et al. 1991, Terekhov et al. 1993, Sazonov et al. 1998). PVO observatory observed a faint gamma-ray emission over ~ 1000 s after the long, 200 s, burst GRB 840304 (Klebesadel 1992). The presence of slowly fading soft gamma-ray (100–500 keV) emission was found in about $\sim 10\%$ of bursts detected by GRANAT/PHEBUS (Tkachenko et al. 1995). Hard gamma-ray photons (0.2–10 GeV) were detected during 1.5 hours after GRB 940217 by EGRET telescope (Hurley et al. 1994).

We present here a detailed analysis of the GRB 920723 light curve, which reveals a soft gamma-ray afterglow with flux decaying as a power law $\sim t^{-0.7}$ during at least 1000 s after the main burst.

2. Observations

SIGMA is the coded-mask telescope with a $15'$ angular resolution operating in the 35–1300 keV energy band (Paul et al. 1991). Typically, SIGMA performs uninterrupted 20–30 h observations, during which the telescope pointing is maintained with a $30'$ accuracy (but known to within $15''$). Although the telescope field of view is only $11.4^\circ \times 10.5^\circ$ (FWHM), some fraction of gamma-rays from sources closer than 35° to the pointing direction reaches the detector through the gaps in the passive shield and produces arc-shaped images. This “secondary optics” (or “sidelobes”) was described in detail by Claret et al. (1994a) along with the appropriate analysis techniques.

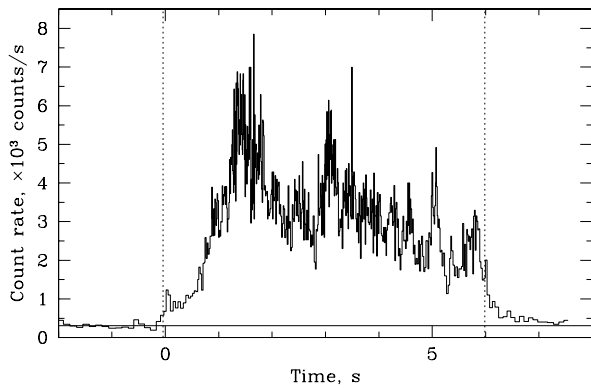


Fig. 1. GRB 920723 light curve with time resolution $\lesssim 0.1$ in 35–300 keV band. The reference time is at the burst trigger. Vertical dotted lines represent the reference times of the light curve in logarithmic coordinates (Fig. 2 and 4).

GRB 920723 was observed by SIGMA through the secondary optics. An $\sim 1^\circ$ localization was obtained from this observation (Claret et al. 1994b). GRB 920723 is one of the brightest bursts observed by GRANAT instruments and the brightest detected by SIGMA. The burst was triggered at $20^{\text{h}}03^{\text{m}}08^{\text{s}}.3$ UT and lasted for about 6 s. The WATCH all-sky monitor provided a 0.2° localization (Sazonov 1998) and observed the fading X-ray emission in the 8–20 keV band during more than 40 s after the main burst (Terekhov et al. 1993). PHEBUS measured the peak burst flux 5×10^{-5} erg s^{-1} cm^{-2} and fluence 1.4×10^{-4} erg cm^{-2} in the 100–500 keV energy band (Terekhov et al. 1995).

The SIGMA data allows the measurements of the burst light curve with better than 0.1 s time resolution (depending on flux) during 7.5 s after the trigger. In addition, the count rate in four wide energy bands (35–70, 70–150, 150–300, 300–600 keV) is recorded with the 4 s time resolution over the entire observation. With these data, it is possible to study the burst emission long after the trigger. Below, we use only the first three energy channels, because the last one is plagued by low sensitivity. The peak burst count rate in the 35–300 keV band was 7900 cnt s^{-1} , much higher than the average background count rate 310 cnt s^{-1} .

During the observation of July 23, 1992, SIGMA was pointed to Her X-1. The pulsar was in eclipse and was not detected. The 3σ upper limit on its 35–70 keV flux averaged over the observation, was 0.25 cnt s^{-1} . The Her X-1 spectrum is known to be very soft (the 20–100 keV photon index is -4.4), and therefore its flux is negligible above 70 keV. The pulsar was in eclipse between 12000 s before the burst and 9000 s after the burst. Therefore, it could not cause any significant variability of the SIGMA count rate during the reported observation. No other known bright sources were visible through either primary or secondary optics of the SIGMA telescope. GRANAT operates on the high apogee orbit and, during the observation, was not influenced by the Earth radiation belts or other magnetospheric anomalies (such as the South Atlantic Anomaly).

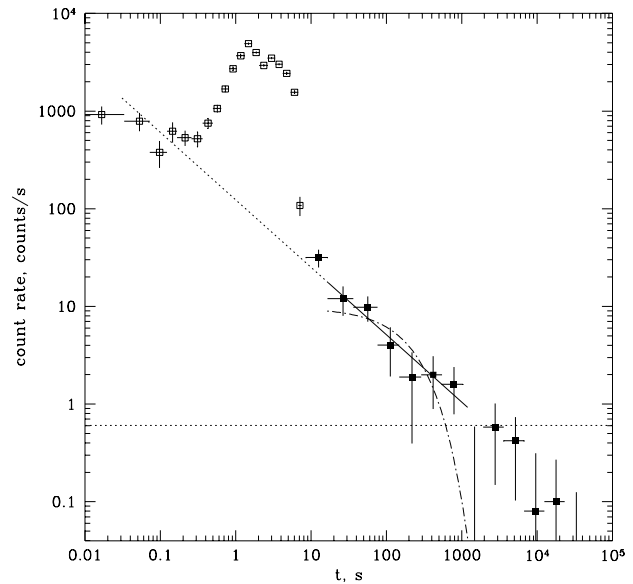


Fig. 2. The background-subtracted burst light curve. Zero time is at the burst trigger. The filled squares show the count rate measured with the 4 s resolution, and the open squares — the data with good time resolution. The horizontal dotted line represents a 95% upper limit on the possible internal background variations on the 300 s time scale (note that Poisson variations are already included in the error bars).

As a result, the SIGMA background usually does not show any significant variations on the time scales shorter than $\sim 10^3$ s. Therefore, it can be accurately modeled by a low degree polynomial.

3. Results

Usually, sources contribute only a small fraction of the total SIGMA count rate. Therefore, the correct background subtraction is vital for the source variability studies. We modeled the background using Chebyshev polynomials. A complete description of the SIGMA background subtraction techniques is presented elsewhere (Burenin et al. 1999); this analysis has shown that the background variations around the subtracted value in excess of Poisson noise are smaller than 0.6 cnt s^{-1} on the 300 s time scale (on the 95% significance level).

Figure 1 shows the burst light curve in the 35–300 keV band. There is a small peak in burst light curve just after the trigger. Within the first second after the trigger, the burst flux rose rapidly. Over the next five seconds, it remained at approximately the same level, showing a strong variability at all resolved time scales. At approximately 6 s after the trigger, the flux started to decline rapidly.

Figure 2 shows the burst light curve in logarithmic coordinates of both time and flux. The shape of the light curve in these coordinates strongly depends on the choice of the reference time. In Fig 2, the reference time is chosen at the moment of the burst trigger. There appears to be a power-law decay of

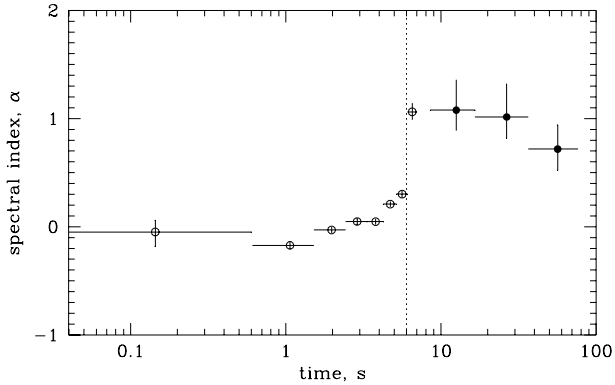


Fig. 3. Time history of the effective spectral index in the 8–200 keV energy band. Zero time is at the burst trigger. Vertical dotted line represents the moment $t = 6$ s from the trigger, when the burst flux began the gradual decline.

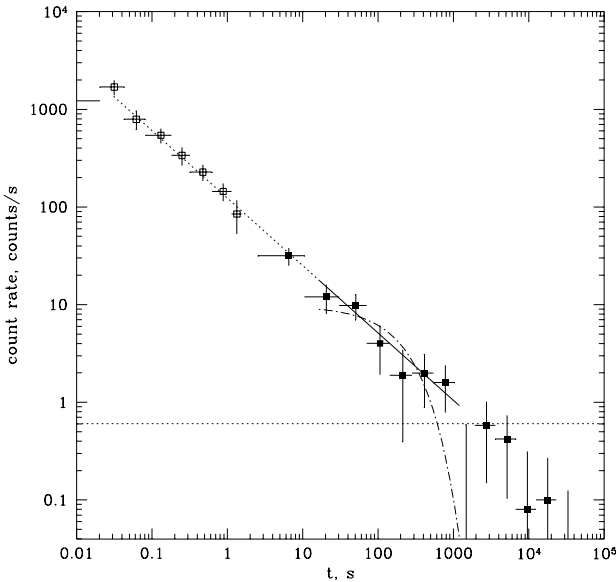


Fig. 4. Same as Fig. 2, but the reference time was set at 6 s after the trigger. The main burst is not shown here because it is at $t < 0$ with this choice of reference time.

flux starting at 10–20 s after the trigger. This behavior is consistent with GRB entering the stage of self-similar fireball expansion soon after the main burst. It should be emphasized that the self-similar behavior is expected only on time scales much larger than those of the main energy release. Therefore, we used the data in the 20–1000 s time interval for the power-law modeling of the light curve.

The solid line in Fig. 2 shows the power law fit in the time interval 20–1000 s; the dash-dotted line shows the exponential fit in the same interval. The reduced χ^2 is 1.5 and 6.5 (4 dof) for the power law and exponential models, respectively. The power law adequately describes the data and results in a better fit than the exponent. The best fit power law index is

-0.69 ± 0.17 ($\Delta\chi^2 = 2.7$ for the index -1). This power law tail contains at least $\sim 20\%$ of the main burst fluence. Applying the same procedure to the three wide energy channels separately, we obtained the power law indices -1.29 ± 0.55 , -0.64 ± 0.19 , and -0.41 ± 0.6 in the 35–70, 70–150, and 150–300 keV energy bands, respectively. Interestingly, the extrapolation of the power law (shown by the dotted line in the Fig. 3) points to the small peak near the beginning of the main burst (Fig. 1).

The spectral evolution of the burst flux can be characterized by the ratio of the 8–20 keV flux measured by WATCH (Terekhov et al. 1993, Sazonov et al. 1998) and the SIGMA flux in the 75–200 keV band. Standard SIGMA calibration does not apply to the secondary optics flux, so we used the PHEBUS measurement of the main burst flux to find the conversion coefficient between SIGMA counts and flux. Figure 3 shows the observed ratio of 8–20 and 75–200 keV fluxes expressed in terms of equivalent spectral index in the 8–200 keV energy range (i.e., the spectral index of an $F_\nu \propto \nu^{-\alpha}$ spectrum with the same hardness ratio as observed). The time behavior of α indicates that the afterglow spectrum is significantly softer than that of the main burst. During the main burst (in the 0–6 s time interval), the usual hard-to-soft evolution of the GRB spectrum is observed (e.g. Ford et al. 1995). Near the start of the gradual decline of the burst flux, 6 s after the trigger (shown by the vertical dotted line in Fig. 1 and 3), α changes abruptly from ≈ 0.3 to ≈ 1 .

It is interesting to examine the light curve with the reference time chosen at $t = 6$ s after the trigger because this moment can be singled out in both flux and spectral history of the burst; the result is presented in Fig. 4. With this choice of zero time, the data in the 0.01–20 s time interval lies on the extrapolation of the power law fit from the 20–1000 s time interval. Adding these data to the fit results in the power law index -0.70 ± 0.03 . Note that in this case, the power law flux decay is observed over approximately four orders of magnitude of time.

4. Discussion

We presented a high sensitivity observation of the GRB 920723 light curve in the soft gamma-ray band. The stable background of SIGMA allows detection of the burst emission on the level of better than 1/1000 of the peak intensity. A similar analysis would be complicated with BATSE because the background is less stable and because the source is eclipsed by Earth every several thousands seconds. We were able to detect the burst afterglow extending up to ~ 1000 s after the main burst. There is a continuous transition of the main burst to its power law afterglow (Fig. 1 and 2). The afterglow spectrum is significantly softer than that of the main burst. An abrupt change in the burst spectrum occurs at approximately the same moment when the power law decay of flux seems to start, at $t \approx 6$ s after the trigger.

The behavior of GRB afterglows in the lower energy bands and at $t \gtrsim 3 \times 10^4$ s can be explained by the synchrotron emission of electrons accelerated in external shocks generated by relativistically expanding fireball colliding with the interstel-

lar medium (e.g. Wijers et al. 1997, Waxman 1997, Sari et al. 1998, Wijers and Galama 1998). In the framework of this model, the spectral flux at the observed frequency ν is given by $F_\nu \propto \nu^{-\alpha} t^{-\beta}$, where α and β are constant and depend only on the spectral index of electrons on sufficiently late stages of the fireball evolution. For GRB 920723 we obtain $\alpha = 1 \pm 0.2$ and $\beta = 0.69 \pm 0.17$. Both the spectrum and the light curve of GRB 920723 seem to be considerably flatter than that of X-ray afterglows observed for other gamma-ray bursts at $t > 3 \times 10^4$ s — $\alpha = 1.4\text{--}1.7$ and $\beta = 1.1\text{--}1.6$ (e.g., in't Zand et al. 1998, Piro et al. 1998, Nicastro et al. 1998). Furthermore, the flux decay observed by SIGMA is flatter than t^{-1} (at $\sim 90\%$ confidence), i.e. the total flux diverges if extrapolated to $t \rightarrow \infty$. This suggests that the afterglow light curve should steepen at some moment during or after the SIGMA observation.

In the relativistic fireball model, the afterglow light curve and the energy spectrum should steepen simultaneously at the moment t_m when the maximum in the electron spectrum, E_m , passes through the SIGMA bandpass (we assume below that t_m corresponds to $E_m = 100$ keV). At later stages of the fireball evolution, indices α and β do not change with time. Since the light curve steepening after 100–1000 s is required by our data at $\sim 90\%$ confidence, it can be suggested that $t_m > 100\text{--}1000$ s. Also, if indeed t_m is > 100 s, our flat spectrum may become consistent with the parameters of X-ray afterglows (see above) because the spectrum softens after t_m . In the adiabatic fireball, t_m can be estimated as $t_m \approx 140 \varepsilon_B^{1/3} \varepsilon_e^{4/3} E_{53}^{1/3}$ s, where $E_{53} \times 10^{53}$ ergs is the total energy release, and $\varepsilon_e < 1$ and $\varepsilon_B < 1$ are the fractions of the electron and magnetic field energy in the total shock energy, respectively (Sari et al. 1998). The value of t_m not much less than 100 s would not be strongly inconsistent with the SIGMA data. However, using ε_e and ε_B estimates from the parameters of radio, optical, and X-ray afterglows of GRB 970508 and GRB 971214 at $t \sim 10^5\text{--}10^6$ s (Wijers & Galama 1998), we obtain $t_m \sim 3$ s, which does seem to contradict our data at $\sim 90\%$ confidence level. This may indicate a large diversity of the fireball parameters in different bursts or some problems of a simple model of a spherically symmetric fireball in explaining the early stages of the gamma-ray burst afterglows.

SIGMA data provides the first convincing observation of the power law afterglow in the soft gamma-rays and immediately after the burst. A very important issue is whether such afterglows are common. A preliminary analysis of other SIGMA bursts revealed no other convincing afterglows, primarily because of the faintness of other bursts; on the basis of SIGMA data alone, we cannot rule out that the soft gamma-ray afterglow is a common phenomenon. A preliminary analysis of the PHEBUS data confirms the detection of the afterglow in GRB 920723 and reveals a similar afterglow in GRB 910402 (Tkachenko et al. 1998). The results of our systematic search for soft gamma-ray afterglows in the GRANAT data will be presented in the future.

5. Acknowledgments

This work was supported by RBRF grants 96–02–18458 and 96–15–96930.

References

- Bloom J. S. et al. 1998, ApJ, in press. (astro-ph/9807315)
 Burenin R. et al. 1999, AstL, in press.
 Claret A. et al. 1994a, A&A, 282, 1034.
 Claret A. et al. 1994b, A&A, 287, 824.
 Costa E. et al. 1997, Nature, 387, 783.
 Djorgovski S. G. et al. 1998, GCN Circ. No. 139
 Frail D.A. et al. 1997, Nature, 389, 261.
 Ford L.A. et al. 1995, ApJ, 439, 307.
 Hurley K. et al. 1994, Nature, 372, 652.
 Klebesadel R. W. 1992, Gamma-Ray Bursts — Observations, analyses and theories, (ed. Ho C., Epstein R., Fenimore E.), Cambridge: Cambridge Univ. Press, P. 161.
 Kulkarni S. R. et al. 1998, Nature, 393, 35.
 Mészáros P., Rees M. 1993, ApJ, 415, 181.
 Mészáros P. 1997, 4th Huntsville Gamma-Ray Bursts Symposium, (astro-ph/9711354).
 Meegan C.A. et al. 1996, ApJS, 106, 65.
 Murakami T. et al. 1991, Nature 350, 592.
 Nicastro L. et al. 1998 A&A, 338, L17.
 Paul J. et al. 1991, Adv. Space Res., 11, No. 8, 289.
 Piro L. et al. 1998, A&A, 331, L41.
 Sazonov S. Yu. et al. 1998, A&A Suppl., 129, 1.
 Sari R. et al. 1998, ApJ, 497, L17.
 Sokolov V.V. et al. 1998, A&A, 334, 117.
 Sunyaev R. et al. 1990, 21st International Cosmic Ray Conference, Conference papers, (ed. Protheroe R.J.), University of Adelaide, V. 12, P. 39.
 Terekhov O. V. et al. 1993, Astron. Lett., 19, 276.
 Terekhov O. V. et al. 1995, Astron. Lett., 21, 73.
 Tkachenko A. et al. 1995, Astrophys Space Sci, 231, 131.
 Tkachenko A., et al. 1998, 3-d INTEGRAL Workshop, in press.
 Van Paradijs J. et al. 1997, Nature, 386, 686.
 Waxman E. 1997, ApJ, 485, L5.
 Wijers R., Rees M., Mészáros P. 1997, MNRAS, 228, L51.
 Wijers R., Galama T. 1998, ApJ, in press. (astro-ph/9805341)
 in't Zand J. J. M. et al. 1998, ApJL, 505, L119.

Appendix A: Background modeling

(This section does not appear in the Journal version)

We start with fitting the background by the Chebyshev polynomial. We exclude the data between 1000 s before the burst and 4000 s after the burst. We increase the order of the polynomial until the F-test indicates that no additional powers of t are necessary; we find that the polynomials of the second and third orders are required to describe the background in spectral channels 1&2 and 3, respectively.

Since the fit is made for the entire observation, the uncertainty of the fit value, arising from statistical uncertainties in the polynomial coefficients, is negligible in any small part of the observation — at least compared to the statistical error of

flux in that part. So, we do not consider the fit uncertainties any further.

The deviations of the data from the fit should ideally be Poissonian. However, we cannot exclude a priori the existence of internal background variations on any time scale. So, we want to place an upper limit on such internal variations. We proceed as follows.

a) We choose the time scale 300 s for this study because this is the width of time bins near 1000 s in Fig. 2 and 3.

b) We average the observed flux in the 300 s bins and make a histogram of deviations from the fit expressed in units of Poisson error in this bin. In the absence of internal variations, this histogram should be consistent with the Gaussian with zero mean and standard deviation = 1 (i.e., with the normal distribution).

c) We do find that the histogram can be described by normal distribution. This shows that there are no biases in the background determination and that the internal background variations on the 300s time scale are small. To set the upper limit, we fit the width of the distribution and then convert the upper limit of the width into the corresponding count rate, assuming that internal variations (if any) and Poisson noise were added in quadrature.

This technique results in a 95% limit of 0.6 cnt/s for internal background variations on the 300 s time scale.